ADVANCED ELECTRONIC MATERIALS
www.advelectronicmat.de

Control of the Schottky Barrier and Contact Resistance at Metal–WSe_2 Interfaces by Polymeric Doping

*Tien Dat Ngo, Myeongjin Lee, Zheng Yang, Fida Ali, Inyong Moon, and Won Jong Yoo**

Tungsten diselenide (WSe_2) is attracting attention because of its superior electronic and optoelectronic properties. In recent years, the number of research works related to the WSe_2-based field-effect transistors (FETs) has increased dramatically. Nonetheless, the performance of 2D WSe_2 is influenced sensitively by metal–semiconductor (MS) interface states, where Fermi-level pinning is substantial. This research explores Fermi-level depinning by doping with an n-type polymer. In this work, spin-coated polyvinyl alcohol (PVA) is used as an n-type dopant for achieving low-contact-resistance WSe_2 FETs in cases of both high-work-function (Pd) and low-work-function (In) metals. Interestingly, the increase in the Schottky barrier height resulting from the application of PVA gives rise to Fowler–Nordheim tunneling for a doped Pd-WSe_2 contact. By contrast, only direct tunneling is observed for an In-WSe_2 contact irrespective of whether the dopant is used. The barrier-height modification after doping reveals that the improvement of the contact resistance is correlated to the enhancement of tunneling current after doping, which is consistent with the measurement results. This work suggests a practical direction for contact engineering of future WSe_2-based electronic devices and expands the current understanding of charge transport at the MS contact when a polymeric n-type dopant is applied.

1. Introduction

Transition-metal dichalcogenides (TMDCs), which exhibit outstanding electrical and optical properties,[1] are attracting increasing interest among the electronic-device research community because of their ultrathinness, which enables efficient low-voltage electrostatic gating, potentially overcoming the limitations of conventional Si technology, e.g., short channel effects and high power generation. Among the TMDCs, WSe_2 has been studied as one of the most promising 2D materials with a sizeable bandgap, high on–off ratio, and compatibility with large-scale chemical vapor deposition synthesis.[2–4] Furthermore, the ability to fabricate WSe_2 surfaces without dangling bonds introduces the possibility of weak van der Waals bonding with other 2D materials, leading to novel electronic and photonic properties of the thus-fabricated heterostructured devices, which can accommodate various materials via stacking. With respect to future applications, WSe_2 exhibits strong potential to be used in field-effect transistors (FETs), photodetectors, light-emitting diodes, and solar cells.[5–9]

The metal–semiconductor (MS) interface is a critical factor influencing the electronic performance of 2D WSe_2 devices in that it is strongly correlated to device polarity.[10] Thus, the Schottky barrier height (SBH) is also an important parameter of the MS interface. In principle, the SBH can be determined according to the Schottky–Mott rule as the difference between the metal work function and the conduction-band edge or valence-band edge for n-type or p-type transistors, respectively.[11,12] However, the SBH in an actual device deviates from the Schottky–Mott rule because of the interfacial energy states.[13] This phenomenon is known as Fermi-level pinning (FLP), and the extent of FLP is quantified by the pinning factor. The pinning factor takes a value from $S = 1$ for no pinning to $S = 0$ for complete pinning. Thus, a novel method is needed to alleviate the FLP of 2D WSe_2 devices and to control their carrier transport properties. Recently, various methods have been proposed to control the FLP of 2D materials, including transferring preformed metals instead of depositing them by evaporation[14,15] and using the edge contact.[16] Nevertheless, most of the proposed techniques involve complicated processes with poorly reproducible results. Here, a polymer-based dopant is introduced for contact engineering because of its convenience, low processing cost, and reliability.

In this work, we attempted to elucidate the effect of a polymeric n-type dopant on the contact properties of WSe_2 devices, focusing on modulating the potential barrier of the MS interface, and thereby the transport mechanism, to promote tunneling current at the MS interface. This idea was proposed for TMDCs in previous research;[17,18] however, no experimental results have been reported to support it for WSe_2. To achieve this objective, we used spin-coated polyvinyl alcohol (PVA) as the dopant for WSe_2 FETs with low- and high-work-function metals (In and Pd, respectively) to demonstrate a clear difference in the transformation of the potential barrier structure. We demonstrate the transition of the potential barriers at the MS interface by measuring the SBH before and after doping. To clarify the results of our SBH measurements, we characterized

T. D. Ngo, M. Lee, Dr. Z. Yang, F. Ali, Dr. I. Moon, Prof. W. J. Yoo
SKKU Advanced Institute of Nano-Technology (SAINT)
Sungkyunkwan University
2066, Seobu-ro, Jangan-gu, Suwon, Gyeonggi-do 16419, South Korea
E-mail: yoowj@skku.edu

The ORCID identification number(s) for the author(s) of this article can be found under https://doi.org/10.1002/aelm.202000616.

DOI: 10.1002/aelm.202000616

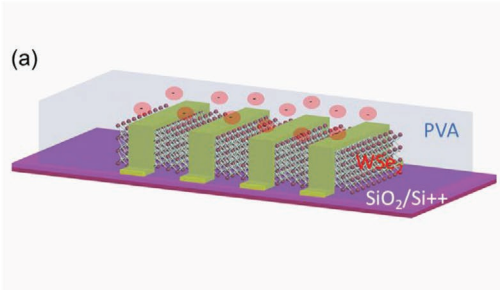

Figure 1. a) Schematic of a WSe_2 FET with PVA coating fabricated on a Si/SiO$_2$ (285 nm) substrate and the transfer length at the interface in the WSe_2 device. b) Cross-sectional view of WSe_2 FET with PVA coating with current crowding near the edge of at the metal interface.

the tunneling behavior at the MS interface, revealing the transition from direct tunneling to Fowler–Nordheim (F–N) tunneling after of PVA onto the Pd-WSe_2 contact; this transition is attributed to the modification of the barrier. By contrast, we observed that only direct tunneling occurred before and after doping for the In-WSe_2 contact. Moreover, we measured the contact resistance before and after doping to demonstrate the influence of barrier modulation by an n-type polymeric dopant on the performance of the device.

2. Results and Discussion

A schematic of a WSe_2 bottom-gate device with PVA encapsulation is shown in **Figure 1**a. Few-layer WSe_2 flakes (thinner than 15 nm) were mechanically exfoliated from bulk WSe_2 using Scotch tape and transferred onto a highly p-doped Si that served as the global bottom-gate substrate capped with a 285 nm thick layer of SiO_2. Thin WSe_2 flakes were observed using an optical microscope. The electrodes were patterned by electron-beam lithography (EBL) and deposited by electron-beam evaporation. The device was initially characterized to confirm its pristine electrical performance. The device was then encapsulated with a 10% PVA solution by spin coating at 4000 rpm and subsequently dried in a vacuum desiccator. The thickness of PVA layer shown in Figure S1 in the Supporting Information is ≈370 nm. The spectral response of Raman shifts photoluminescence (PL) of WSe_2 before and after doping is shown in Figure S2 in the Supporting Information which reveals the effective n-type doping from PVA.

The band structure of PVA has been reported in ref. [19]. Electron injection at the interface between PVA and 2D materials due to the hydroxyl group (–OH) in PVA behaving as an electron donor has also been reported.[20,21] The efficiency of electron injection of PVA depends on the doping concentration. The transfer characteristics of a 2D material increased when PVA with higher doping concentration was applied.[20] The method to estimate doping concentration before and after doping is detailed in Figure S3 in the Supporting Information. Moreover, the stability of the device with higher doping concentration has also been reported.[22] In our work, as a result of the difference in electron affinity between PVA and WSe_2 (the conduction-band edge of monolayer WSe_2 is ≈–3.5 to −3.9 eV from the vacuum level[23]), the n-type doping effect is induced by bottom-gating with PVA encapsulation. **Figure 2**a,b shows the transfer curves of the pristine and doped WSe_2 devices with different metal contacts at $V_D = 1$ V. Indium (In) and palladium (Pd) were chosen because they are expected to form low and high SBHs with WSe_2, respectively. In has a relatively low work function of ≈4.5 eV and exhibits good Ohmic contact with WSe_2,[24] whereas Pd is a high-work-function metal (≈5.2 eV) suitable for preparing p-type FETs.[14] With this difference in work functions, we can clearly distinguish the transformation of the barrier formed at the MS interface by using the n-type dopant. We also fabricated Ti-contact (as another metal with a low work function) device to confirm the doping effect of PVA on WSe_2 (Figure S4, Supporting Information). Both the pristine WSe_2 device with a Pd contact and that with an In contact demonstrate ambipolar behavior with stronger n-type characteristics, revealing strong FLP because of the interface states at the metal–WSe_2 contact, which is consistent with previous research.[25] However, the intrinsic WSe_2 FET with an In contact exhibits a higher on–off ratio and higher on-state current than that with a Pd contact (10^7 vs 10^5). Moreover, the output curves of the devices demonstrate Ohmic-type contact for the In-WSe_2 device and typical Schottky contact behavior for the Pd-WSe_2 device. After the PVA coating is applied, both devices show improvement in their on-state currents. We observe an approximately one-order increase in the maximum on-state and a negative voltage shift of the threshold voltage of ≈15 V for the Pd-contact device. A similar trend is observed for the In-contact device (the on-state current increases from 140 to 190 μA and the threshold exhibits a negative shift of ≈30 V). Nevertheless, we observed that the off-state current of the devices remains low, which contributes to the increase of the on–off ratio. This trend is opposite that observed for other degenerate chemical dopants reported refs. [18, 26]. This difference reveals an n-type nondegenerate doping effect of PVA for the WSe_2 bottom-gate device. Interestingly, the output curve of the Pd-WSe_2 device becomes more linear than that of the intrinsic device, which indicates Ohmic-like contact after doping (Figure 2b and Figure S5, Supporting Information). On the basis of the modification of the properties of the contact, we speculate that the MS interface of the WSe_2 FETs is modulated by the n-type polymeric dopant.

To explain the results, we measured the SBH for both the In-contact and Pd-contact devices before and after doping. The SBH for n-type semiconductors is determined by the difference between the work function of the metal and the conduction-band edge of the semiconductor. For a Schottky-contact device,

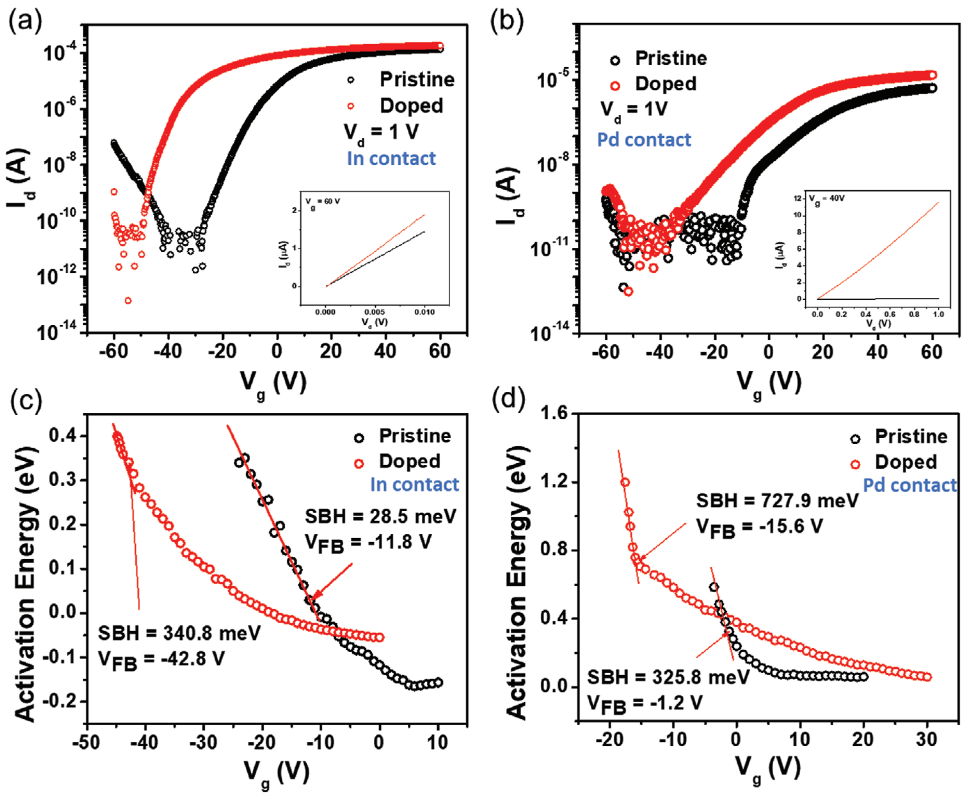

Figure 2. a,b) Transfer curves of In and Pd devices before and after doping (inset: output curve of In and Pd devices before and after doping). c,d) Schottky barrier height of the device before and after doping.

the current that can cross SBH can be expressed by the following thermionic emission equations[27]

$$I_{2D} = WA^*_{2D}T^{\frac{3}{2}} \exp\left(-\frac{q\phi_{Bn}}{kT}\right) exp\left(\frac{qV_D}{kT}\right), A^*_{2D} = \frac{q\sqrt{8\pi m^* k^3}}{h^2} \quad (1)$$

$$\phi_{Bn} = \frac{k}{q}\left[-\frac{\Delta \ln\left(I_D / T^{\frac{3}{2}}\right)}{\Delta T^{-1}}\right] \quad (2)$$

where W is the channel width, k is the Boltzmann constant, q is the electron charge, A^*_{2D} is the modified Richardson constant, ϕ_{Bn} is the SBH, m^* is the effective mass, h is Planck's constant, and V_D is the drain voltage. Equation (2) is derived from Equation (1) for extracting the SBH. Thus, we can measure the SBH of the device using data obtained from temperature-dependent transfer curves. We applied V_D = 1 V for all of the investigated WSe_2 devices. From Equation (2), we acquired the negative slope from the linear fit of the value of ln $(I_D/T^{3/2})$ as a function of k/qT. Note that the flat-band voltage (V_{FB}) is the threshold gate bias at which the transport of the device occurs by thermionic emission alone. That is, the determination of SBH is inappropriate when $V_G > V_{FB}$ as the current that tunnels through the SBH is generated. As a result, the SBH measured at $V_G = V_{FB}$ becomes the true SBH at the WSe_2–metal contact. In the present work, we conducted high-temperature measurements for extracting the SBH because the thermionic current is enhanced at high temperatures; therefore, the results can be more accurate than those corresponding to low temperatures.[28] In our experiments, the maximum temperature that we use is 150 °C because the melting point of PVA is ≈220 °C.[29] Moreover, the PVA becomes more stable due to the increase in crystallinity after the utilization of appropriate annealing.[30–33]

On the basis of the aforementioned assumption, we extracted SBH as a function of the gate bias for the In- and Pd-contact devices before and after doping, as shown in Figure 2c,d. The temperature dependence of IV characteristic of devices is in Figures S6 and S9 in the Supporting Information. For the intrinsic In- and Pd-contact devices, the SBH were found to be 28.5 meV at V_G = −11.8 V and 325.8 meV at V_G = −1.2 V, respectively; these values are proportional to the difference between the metal work functions of In and Pd and the conduction-band edge of WSe_2. After doping, the SBH of the In-contact device increases tenfold to 340.8 meV, whereas that of the Pd-contact device increases twofold to 727.9 meV. To confirm the reproducibility of the increase in SBH, the two different devices were tested again; the results for Pd-WSe_2 are shown in Figures S7 and S8 in the Supporting Information, and that for In-WSe_2 is shown in Figure S10 in the Supporting Information.

We explain the mechanism behind the observed tendency using the band diagram plotted in **Figure 3**. In the ideal case, the SBH of the In-WSe_2 device is the difference between the conduction-band edge and the Fermi level of In. For Pd-WSe_2,

ADVANCED ELECTRONIC MATERIALS
www.advelectronicmat.de

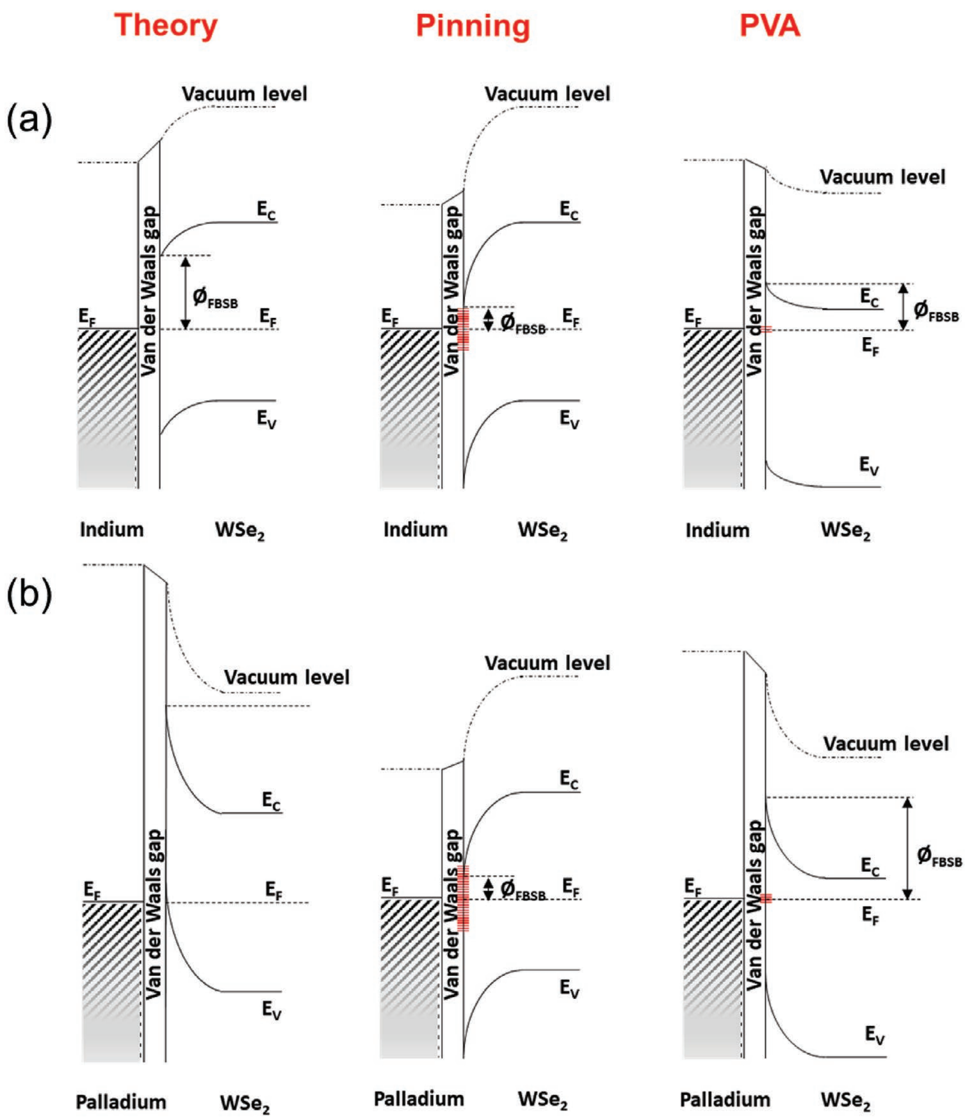

Figure 3. Band diagrams with no pinning before doping, with pinning before doping, and without pinning after doping a) for the In contact device and b) for the Pd contact device.

after the contact is formed, the Fermi level of Pd is located at the valence-band edge of WSe_2. Thus, in the ideal case, the Pd-WSe_2 device would demonstrate p-type electronic behavior and the SBH would not change when we apply a dopant to the device. Nonetheless, our experimental results indicated strong FLP at the MS contact. For the actual devices, the SBH of both types of devices is pinned near the conduction-band edge, which explains the n-type behavior of the Pd-WSe_2 device. The FLP effect of our devices is consistent with previous reports related to 2D TMDCs.[28,34] This phenomenon arises from the additional charge traps introduced during the evaporation process or from the intrinsic defects which are known as interface states of the 2D materials perturbing the orbital overlap at the MS interface and therefore changing the electronic structures.[35–37] This phenomenon was confirmed for WSe_2 in previous research.[38,39] Moreover, the metal-like defects at the MS contact have been recently reported to contribute to the strong pinning of the barrier at the MS interface.[40] Because of the charged nature of these defects and states, they can be screened by the dielectric dipole or by the stronger charged cloud. When n-type dopants are used, the carrier density of a semiconductor at the transfer length increases. Even though we spin-coated PVA on the surface of the device, the electron can diffuse to the transfer length. Recently, Pang et al. reported that surface dopants diffuse to the transfer length of devices even with the hard mask used for the electrical contact region.[41] Besides, they also reported the Fermi-level depinning by p-type doping.[42] Moreover, PVA as a dielectric layer provides a screening effect to long-range charge scattering, alleviating FLP.[43] Using Figure 2a, we estimate the density of interface states before and after doping, confirming its decrease after PVA is applied (see Figure S11, Supporting Information). Notably, the pinning factor of our devices increased after the PVA was applied (Figure S12, Supporting Information), indicating that the Fermi level was depinned. This depinning induces a change in the structure of the barrier, enabling a substantial increase in tunneling. To comprehensively determine the influence of the Fermi-level depinning induced by a polymeric n-type dopant on the properties of the metal–WSe_2 contact, the tunneling transport mechanism of the device should be investigated because tunneling becomes the main transport mechanism as a result of the enhancement in barrier height of the contact formed by dopants.[10] Moreover, by extracting the tunneling transport which consists of F–N tunneling and direct tunneling, we attain a clear view of the barrier structure before and after doping. When the barrier at the interface is triangular-shaped, the F–N tunneling takes place because electrons can tunnel through the sufficiently thin barrier; however, when the barrier is trapezoidal-shaped, the direct tunneling takes place through the barrier instead. From Equations (6) and (8) in Figure S13 in the Supporting Information, we understand that the plot of ln (I/V^2) versus $1/V$ demonstrates the logarithmic dependence when the direct tunneling takes place, while with F–N tunneling it shows the linear dependence with negative slope when the applied bias is close to the barrier height[44,45] or the doping level is sufficiently high for inducing a barrier height. The I–V characteristics of the Pd-contact devices before and after doping are shown in **Figure 4**c,d. We observed the transition from direct tunneling to F–N tunneling after PVA was doped onto the Pd-WSe_2 contact, which we attributed to modification of the barrier. The results show a triangular shape of the barrier after the PVA was applied, which is consistent with Figure 4b.

The increasing trend of SBH after doping causes the suppression of the thermionic emission of the charge through the barrier. However, as previously discussed, the transformation of the barrier structure contributes to the domination of electrons tunneling through the barrier. Thus, we measured the contact resistance of the device to confirm the improvement of the contact through Fermi-level depinning. In many 2D devices, contact resistance dominates device performance. To investigate the contact resistance of WSe_2 devices influenced by n-type dopants, we carried out four-point probe (4pp) measurements. The device configuration for the 4pp measurements is shown in Figure S14e in the Supporting Information. The extraction of the contact resistance from the 4pp measurements before and after doping is described in Figure S14 in the Supporting Information. Figure S14a–d in the Supporting Information shows the results obtained from the 4pp measurement. The intrinsic contact resistance of the In-contact device measured at 60 V (52.5 kΩ μm) is substantially lower than that of the intrinsic Pd-contact device (1442 kΩ μm). For the intrinsic In-contact device, the ratio between the contact resistance and the total resistance is 29.2% at V_G = 60 V (Figure 4e). The small value of this ratio indicates that sheet resistance dominates the device performance. Thus, this low contact resistance of the intrinsic In-contact device supports the results of a previous report on the role of metals in WSe_2 FETs.[24] By contrast, the intrinsic Pd-contact device exhibits the opposite trend; the contact resistance

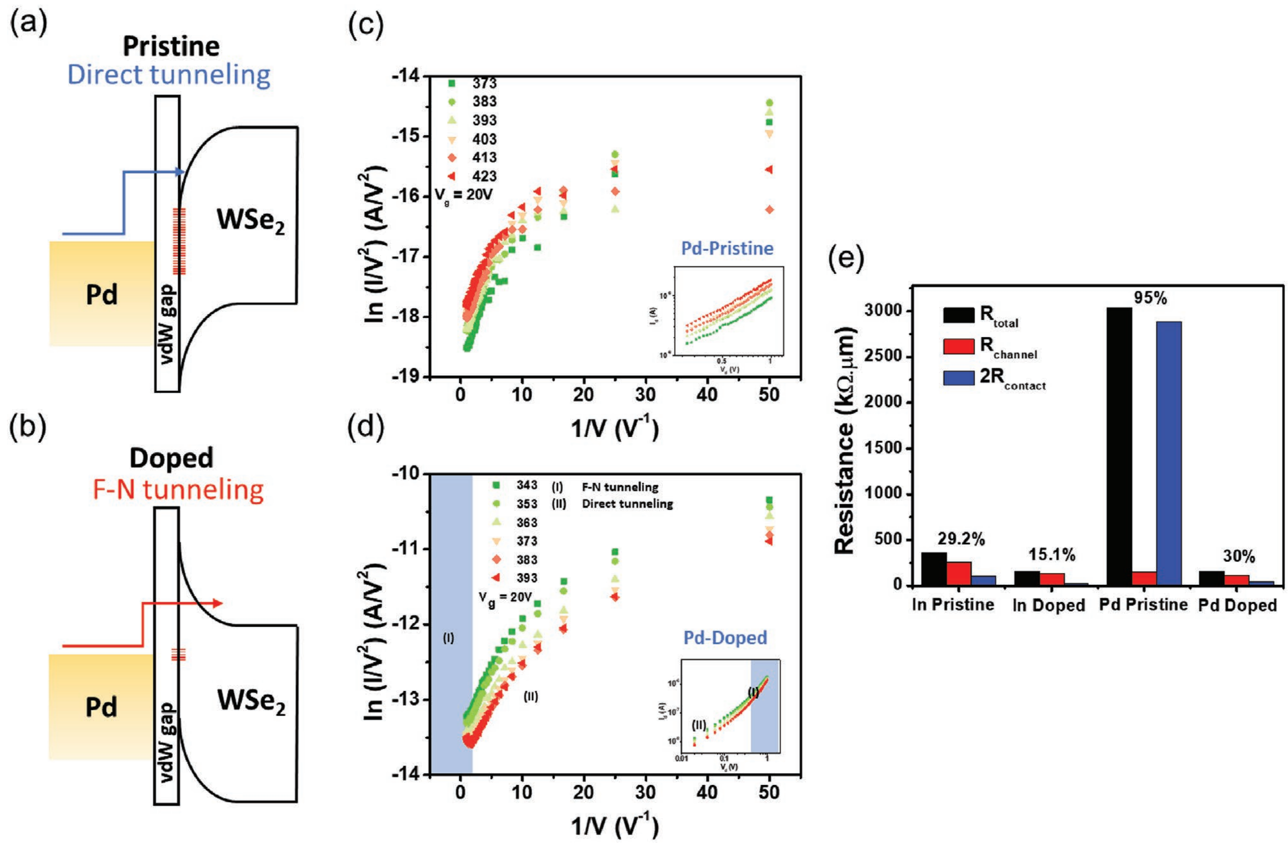

Figure 4. a,b) Band diagrams showing the tunneling mechanism of Pd-WSe_2 contact device before and after doping, respectively. c,d) $\ln(I/V^2)$ plotted as a function of the inverse of drain bias ($1/V$) for the Pd contact device before and after doping, respectively. Insets show the log–log scale output curves. e) Percentages of the contact resistance with respect to the total resistance of In-WSe_2 and Pd-WSe_2 contact devices before and after doping.

governs the device operation, with a high ratio with respect to the total resistance. Therefore, we propose that In is a better contact material than Pd for pristine WSe_2 devices.

In addition, even though Ti is also a low-work-function metal, the contact resistance of the intrinsic Ti-contact device is still relatively high compared with that of the intrinsic In-contact device (Figure S4c, Supporting Information). These results related to high and low work functions were predicted in previous theoretical work.[46] After the doping with PVA, we observed a dramatic decrease in contact resistance of both the In and Pd contacts. For the In-contact device, the minimum contact resistance decreases by one order after doping. Likewise, the Pd contact device demonstrates an approximately two-order reduction in contact resistance after doping. Moreover, the contact resistance ratio of the Pd-contact device decreases substantially, from 95% to 30%, at V_G = 60 V, confirming that n-type doping of the channel improves the contact property of the device. This phenomenon originates from the transition in the barrier structure at the MS interface of WSe_2 devices because of n-type dopants, giving rise to an increase in the number of electrons that tunnel through the barrier. This mechanism has previously been used to explain the good Ohmic contact induced by ion implantation, which has been widely used in conventional semiconductors.[17]

In addition to the experimental results, we performed numerical calculations for the current components shown in Figure S15b in the Supporting Information for both the In- and Pd-contact devices. We used an analytical model that includes the three current components.[44,47] We extracted the current components (Figure S15c,d, Supporting Information) that contribute to the carrier transport of the WSe_2 device with PVA applied. From this numerical calculation, we confirm that n-type doping is the cause of the reduction of the thermionic current and the generation of the tunneling current because of the barrier modulation.

3. Conclusion

We revealed the depinning effect at the MS interface of WSe_2 FETs by using a very practical polymeric doping method. By interpreting the charge transport at the metal–2D interface on the basis of experimental and simulation results, we found that the barrier structure of the MS interface and corresponding tunneling are the origin of the improvement in the In- and Pd-contact properties when PVA-induced n-type dopants are applied. This work demonstrates the feasibility of the polymeric doping technique in the development of reliable 2D devices.

4. Experimental Section

Fabrication of Pristine WSe2 FETs: The WSe_2 thin flakes (thinner than 15 nm) were mechanically exfoliated from bulk WSe_2 using Scotch tape. Prior to device fabrication, the heavily doped p-type Si wafers with SiO_2 as the dielectric layer (with a thickness of 285 nm) were cleaned thoroughly in acetone and isopropyl alcohol in a sonicator for 20 min. The pristine few-layer thick WSe_2 was transferred onto a p-type Si/SiO_2 substrate. The WSe_2 flakes were identified using an optical microscope. The metal contacts were patterned by EBL and a metal electrode of Pd (20/50 nm) or In (20/50) was deposited using electron-beam deposition.

Preparation of PVA: PVA was dissolved in dimethyl sulfoxide. The solution was mixed by magnetic stirring at 80 °C for 12 h to enhance its homogeneity. The WSe_2 was doped by spin coating at 4000 rpm in 60 s. The samples were stored in a vacuum desiccator for 2 h to remove the solvent and annealed at 150 °C for half an hour on the hot plate.

Device Characterization—Optical, Raman, and Photoluminescence Measurements: All of the optical images of the WSe_2 devices were obtained using a microscope equipped with a video camera. The Raman and PL measurements were conducted with a micro-Raman spectroscopy system equipped with 532 nm laser (spot size ≈ 1 µm) operated at 0.2 mW laser power and a Xe-arc-lamp-equipped fluorometer with a power of 0.2 mW.

Device Characterization—Electrical Measurements: All of the electrical measurements were performed using a semiconductor parameter analyzer connected to a 20 mTorr vacuum probe station.

Device Characterization—Atomic Force Microscope (AFM): The thickness of the PVA layer was measured by using AFM. AFM was performed by placing the sample on a metal puck, which was connected to the ground. The AFM image was taken at room temperature under atmospheric pressure and dehumidification condition (<25%) under noncontact mode.

Supporting Information

Supporting Information is available from the Wiley Online Library or from the author.

Acknowledgements

This work was supported by the Global Research Laboratory (GRL) Program (2016K1A1A2912707) funded by National Research Foundation of Korea (NRF).

Conflict of Interest

The authors declare no conflict of interest.

Keywords

contact resistance, fermi level depinning, n-type doping, polyvinyl alcohol, tungsten diselenide

Received: June 15, 2020
Revised: July 23, 2020
Published online:

[1] K. S. Novoselov, A. K. Geim, S. V. Morozov, D. Jiang, Y. Zhang, S. V. Dubonos, I. V. Grigorieva, A. A. Firsov, *Science* **2004**, *306*, 666.
[2] B. Liu, M. Fathi, L. Chen, A. Abbas, Y. Ma, C. Zhou, *ACS Nano* **2015**, *9*, 6119.
[3] X. Wang, Y. Li, L. Zhuo, J. Zheng, X. Peng, Z. Jiao, X. Xiong, J. Han, W. Xiao, *CrystEngComm* **2018**, *20*, 6267.
[4] H. Jiang, *J. Phys. Chem. C* **2012**, *116*, 7664.
[5] J. S. Ross, P. Klement, A. M. Jones, N. J. Ghimire, J. Yan, D. G. Mandrus, T. Taniguchi, K. Watanabe, K. Kitamura, W. Yao, D. H. Cobden, X. Xu, *Nat. Nanotechnol.* **2014**, *9*, 268.

[6] D. A. Nguyen, H. M. Oh, N. T. Duong, S. Bang, S. J. Yoon, M. S. Jeong, *ACS Appl. Mater. Interfaces* **2018**, *10*, 10322.
[7] B. W. H. Baugher, H. O. H. Churchill, Y. Yang, P. Jarillo-Herrero, *Nat. Nanotechnol.* **2014**, *9*, 262.
[8] C. Park, N. T. Duong, S. Bang, D. A. Nguyen, H. M. Oh, M. S. Jeong, *Nanoscale* **2018**, *10*, 20306.
[9] A. Pospischil, M. M. Furchi, T. Mueller, *Nat. Nanotechnol.* **2014**, *9*, 257.
[10] S. M. Sze, K. K. Ng, *Physics of Semiconductor Devices Physics of Semiconductor Devices*, 3rd ed., Wiley, New York **1995**, pp. 134–196.
[11] N. F. Mott, *Proc. R. Soc. London, Ser. A* **1939**, *171*, 27.
[12] W. Schottky, *Naturwissenschaften* **1938**, *26*, 843.
[13] J. Bardeen, *Phys. Rev.* **1947**, *71*, 717.
[14] Y. Jung, M. S. Choi, A. Nipane, A. Borah, B. Kim, A. Zangiabadi, T. Taniguchi, K. Watanabe, W. J. Yoo, J. Hone, J. T. Teherani, *Nat. Electron.* **2019**, *2*, 187.
[15] Y. Liu, J. Guo, E. Zhu, L. Liao, S. J. Lee, M. Ding, I. Shakir, V. Gambin, Y. Huang, X. Duan, *Nature* **2018**, *557*, 696.
[16] Z. Yang, C. Kim, K. Y. Lee, M. Lee, S. Appalakondaiah, C. H. Ra, K. Watanabe, T. Taniguchi, K. Cho, E. Hwang, J. Hone, W. J. Yoo, *Adv. Mater.* **2019**, *31*, 1808231.
[17] A. Allain, J. Kang, K. Banerjee, A. Kis, *Nat. Mater.* **2015**, *14*, 1195.
[18] D. Kiriya, M. Tosun, P. Zhao, J. S. Kang, A. Javey, *J. Am. Chem. Soc.* **2014**, *136*, 7853.
[19] M. K. El-Mansy, E. M. Sheha, K. R. Patel, G. D. Sharma, *Optik* **2013**, *124*, 1624.
[20] C. J. Lockhart De La Rosa, A. Nourbakhsh, M. Heyne, I. Asselberghs, C. Huyghebaert, I. Radu, M. Heyns, S. De Gendt, *Nanoscale* **2017**, *9*, 258.
[21] C. J. Lockhart De La Rosa, G. Arutchelvan, A. Leonhardt, C. Huyghebaert, I. Radu, M. Heyns, S. De Gendt, *APL Mater.* **2018**, *6*, 058301.
[22] S. Kim, P. Zhao, S. Aikawa, E. Einarsson, S. Chiashi, S. Maruyama, *ACS Appl. Mater. Interfaces* **2015**, *7*, 9702.
[23] F. A. Rasmussen, K. S. Thygesen, *J. Phys. Chem. C* **2015**, *119*, 13169.
[24] W. Liu, J. Kang, D. Sarkar, Y. Khatami, D. Jena, K. Banerjee, *Nano Lett.* **2013**, *13*, 1983.
[25] K. Sotthewes, R. Van Bremen, E. Dollekamp, T. Boulogne, K. Nowakowski, D. Kas, H. J. W. Zandvliet, P. Bampoulis, *J. Phys. Chem. C* **2019**, *123*, 5411.
[26] H. Fang, M. Tosun, G. Seol, T. C. Chang, K. Takei, J. Guo, A. Javey, *Nano Lett.* **2013**, *13*, 1991.
[27] A. Anwar, B. Nabet, J. Culp, F. Castro, *J. Appl. Phys.* **1999**, *85*, 2663.
[28] C. Kim, I. Moon, D. Lee, M. S. Choi, F. Ahmed, S. Nam, Y. Cho, H. J. Shin, S. Park, W. J. Yoo, *ACS Nano* **2017**, *11*, 1588.
[29] R. K. Tubbs, *J. Polym. Sci., Part A* **1965**, *3*, 4181.
[30] N. A. Peppas, *Eur. Polym. J.* **1976**, *12*, 495.
[31] T. Terao, S. Maeda, A. Saika, *Macromolecules* **1983**, *16*, 1535.
[32] R. M. Hodge, G. H. Edward, G. P. Simon, *Polymer* **1996**, *37*, 1371.
[33] H. E. Assender, A. H. Windle, *Polymer* **1998**, *39*, 4295.
[34] Y. Guo, D. Liu, J. Robertson, *ACS Appl. Mater. Interfaces* **2015**, *7*, 25709.
[35] S. McDonnell, R. Addou, C. Buie, R. M. Wallace, C. L. Hinkle, *ACS Nano* **2014**, *8*, 2880.
[36] R. Addou, S. McDonnell, D. Barrera, Z. Guo, A. Azcatl, J. Wang, H. Zhu, C. L. Hinkle, M. Quevedo-Lopez, H. N. Alshareef, L. Colombo, J. W. P. Hsu, R. M. Wallace, *ACS Nano* **2015**, *9*, 9124.
[37] R. Addou, L. Colombo, R. M. Wallace, *ACS Appl. Mater. Interfaces* **2015**, *7*, 11921.
[38] C. M. Smyth, R. Addou, S. McDonnell, C. L. Hinkle, R. M. Wallace, *2D Mater.* **2017**, *4*, 025084.
[39] R. Addou, R. M. Wallace, *ACS Appl. Mater. Interfaces* **2016**, *8*, 26400.
[40] P. Bampoulis, R. Van Bremen, Q. Yao, B. Poelsema, H. J. W. Zandvliet, K. Sotthewes, *ACS Appl. Mater. Interfaces* **2017**, *9*, 19278.
[41] C. Pang, T. Y. T. Hung, A. Khosravi, R. Addou, Q. Wang, M. J. Kim, R. M. Wallace, Z. Chen, *Adv. Electron. Mater.* **2020**, *6*, 1901304.
[42] C.-S. Pang, T. Y. T. Hung, A. Khosravi, R. Addou, R. M. Wallace, Z. Chen, *IEEE Electron Device Lett.* **2020**, *41*, 1122.
[43] W. Bao, X. Cai, D. Kim, K. Sridhara, M. S. Fuhrer, *Appl. Phys. Lett.* **2013**, *102*, 042104.
[44] F. Ahmed, M. S. Choi, X. Liu, W. J. Yoo, *Nanoscale* **2015**, *7*, 9222.
[45] M. H. Doan, Y. Jin, S. Adhikari, S. Lee, J. Zhao, S. C. Lim, Y. H. Lee, *ACS Nano* **2017**, *11*, 3832.
[46] J. Kang, W. Liu, D. Sarkar, D. Jena, K. Banerjee, *Phys. Rev. X* **2014**, *4*, 031005.
[47] S. Das, A. Prakash, R. Salazar, J. Appenzeller, *ACS Nano* **2014**, *8*, 1681.

